Journal of Virology

Structurally Similar Woodchuck and Human Hepadnavirus Core Proteins Have Distinctly Different Temperature Dependences of Assembly

Alexander A. Kukreja, Joseph C.-Y. Wang, Elizabeth Pierson, David Z. Keifer, Lisa Selzer, Zhenning Tan, Bogdan Dragnea, Martin F. Jarrold and Adam Zlotnick

J. Virol. **2014, 88(24):14105. DOI: 10.1128/JVI.01840-14.**
Published Ahead of Print 24 September 2014.

JVI Journals.ASM.org

Structurally Similar Woodchuck and Human Hepadnavirus Core Proteins Have Distinctly Different Temperature Dependences of Assembly

Alexander A. Kukreja,[a]* Joseph C.-Y. Wang,[a] Elizabeth Pierson,[b] David Z. Keifer,[b] Lisa Selzer,[a] Zhenning Tan,[a]* Bogdan Dragnea,[b] Martin F. Jarrold,[b] Adam Zlotnick[a]

Department of Molecular and Cellular Biochemistry, Indiana University, Bloomington, Indiana, USA[a]; Department of Chemistry, Indiana University, Bloomington, Indiana, USA[b]

ABSTRACT

Woodchuck hepatitis virus (WHV), a close relative of human hepatitis B virus (HBV), has been a key model for disease progression and clinical studies. Sequences of the assembly domain of WHV and HBV core proteins (wCp149 and hCp149, respectively) have 65% identity, suggesting similar assembly behaviors. We report a cryo-electron microscopy (cryo-EM) structure of the WHV capsid at nanometer resolution and characterization of wCp149 assembly. At this resolution, the T=4 capsid structures of WHV and HBV are practically identical. In contrast to their structural similarity, wCp149 demonstrates enhanced assembly kinetics and stronger dimer-dimer interactions than hCp149: at 23°C and at 100 mM ionic strength, the pseudocritical concentrations of assembly of wCp149 and hCp149 are 1.8 μM and 43.3 μM, respectively. Transmission electron microscopy reveals that wCp149 assembles into predominantly T=4 capsids with a sizeable population of larger, nonicosahedral structures. Charge detection mass spectrometry indicates that T=3 particles are extremely rare compared to the ~5% observed in hCp149 reactions. Unlike hCp149, wCp149 capsid assembly is favorable over a temperature range of 4°C to 37°C; van't Hoff analyses relate the differences in temperature dependence to the high positive values for heat capacity, enthalpy, and entropy of wCp149 assembly. Because the final capsids are so similar, these findings suggest that free wCp149 and hCp149 undergo different structural transitions leading to assembly. The difference in the temperature dependence of wCp149 assembly may be related to the temperature range of its hibernating host.

IMPORTANCE

In this paper, we present a cryo-EM structure of a WHV capsid showing its similarity to HBV. We then observe that the assembly properties of the two homologous proteins are very different. Unlike human HBV, the capsid protein of WHV has evolved to function in a nonhomeostatic environment. These studies yield insight into the interplay between core protein self-assembly and the host environment, which may be particularly relevant to plant viruses and viruses with zoonotic cycles involving insect vectors.

Hepatitis B virus (HBV) infection is widespread, causing chronic infection in 360 million people worldwide and leading to 600,000 deaths annually (1, 2). Current treatments are unable to clear viral infection and are prone to the appearance of drug-resistant mutants (4–8). Efforts to produce better treatments remain an active goal of HBV research. Woodchuck hepatitis virus (WHV) and the woodchuck model system have been key to understanding natural viral infection and to developing antiviral therapies (9–11). In this regard, a better understanding of the WHV model system is desirable.

WHV virions and infections are similar to those of HBV. The viruses have the same genetic organization and complement of proteins and elicit comparable pathogenic responses (10, 11). WHV is an enveloped, icosahedral, partially double-stranded DNA virus encoding a viral reverse transcriptase (P), a structural core protein (Cp), two variants of the envelope protein or surface antigen (S-HBsAg and L-HBsAg; HBV encodes a third surface protein variant, M, that is not required for infection), and a regulatory X protein (12–14). The viral life cycle begins with viral entry through a cell-specific receptor (15), leading to the delivery of the partially double-stranded relaxed circular DNA (rcDNA) to the nucleus. Host enzymes convert rcDNA to covalently closed circular DNA (cccDNA), which serves as the template for viral transcription. A terminally redundant mRNA from cccDNA, the pregenomic RNA (pgRNA), is bound by P, and this complex is packaged by Cp to form a pgRNA-filled capsid. Reverse transcription occurs within the capsid to form rcDNA, at which point capsids can be either recycled to the nucleus or bound by envelope proteins to produce a mature, enveloped virion.

The 183-residue capsid-forming core protein, Cp, has been of particular interest and studied extensively for HBV. Cp is a self-assembling homodimer that forms capsids with predominately T=4 symmetry (i.e., 120 dimers) and ~5% with T=3 symmetry (90 dimers) (16). The protein can be divided into two domains: an assembly domain comprised of the first 149 residues and a 34-residue arginine-rich RNA-binding domain at the C terminus

Received 25 June 2014 Accepted 22 September 2014
Published ahead of print 24 September 2014
Editor: W. I. Sundquist
Address correspondence to Adam Zlotnick, azlotnic@indiana.edu.
* Present address: Alexander A. Kukreja, Department of Biophysics, University of Michigan, Ann Arbor, Michigan, USA; Zhenning Tan, Assembly Biosciences, San Francisco, California, USA.

doi:10.1128/JVI.01840-14

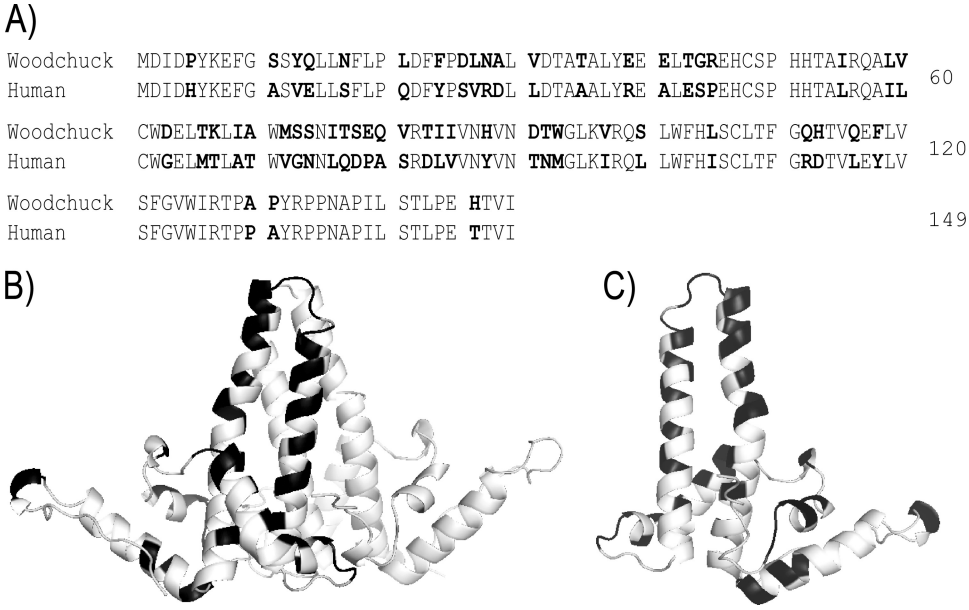

FIG 1 Woodchuck and human core protein assembly domains (residues 1 to 149) show 65% identity. (A) Sequence alignment of wCp149 and hCp149 reveals 97 conserved residues. Differences are highlighted in boldface type. (B) Ribbon diagram of an hCp149 dimer (PDB accession number 1QGT) marked with black residues on one monomer to illustrate the position of sequence differences. The majority of these residues are located at the spike tip, the site of intradimer interactions. (C) The differences in helix 3 (leftmost vertical helix) lie predominately toward the outer surface of the dimer, whereas the differences in helix 4 (the vertical helix on the right) include the intradimer interface.

(17). While unable to package RNA, a truncated HBV Cp containing only the assembly domain (hCp149) has been a useful tool for understanding the self-assembly reaction and capsid formation. *In vitro* experiments have shown that hCp149 assembly is influenced by ionic strength, pH, temperature, and core protein concentrations (18–20). HBV assembly displays sigmoidal kinetics and equilibrates within 24 h. These *in vitro*-assembled particles are morphologically indistinguishable from capsids composed of full-length Cp purified from cell culture (21).

Thermodynamic and kinetic models of HBV capsid assembly have been developed, which recapitulate many of its features, allowing interpretation of assembly data (22–24). Interactions between Cp149 dimers are weak, equivalent to a dissociation constant of 1 mM (−3 to −4 kcal/mol); capsids can assemble because dimers are tetravalent. Stronger interactions lead to kinetic traps from the formation of on- or off-path intermediates that deplete the reaction of free dimer (24). Once assembled, capsids are extremely stable and exhibit a hysteresis to disassembly, allowing capsids to persist under conditions where dimers do not assemble (25). Recent evidence suggests that postassembly transitions may also affect capsid stability (31).

The dynamic nature of hCp149 is further illustrated by several point mutations (e.g., F97L), which modify the assembly behavior of the protein, although they are not at an interdimer interface (27–29). The redox state of a pair of cysteines (C61) located at the intradimer interface, distant from the interdimer interface, also substantially affects assembly properties and capsid stability (30, 31). These data are suggestive of unique structural and assembly behaviors.

In this study, comparison of HBV and WHV reveals important similarities and differences. Sequence alignments of the WHV and HBV assembly domains have 65% identity (Fig. 1A). Modeling of the sequence differences on an hCp149 dimer reveals that most of these differences are on the exposed, spike alpha helices that make up the intradimer interface (Fig. 1B and C). Using the assembly domain of the WHV core protein (wCp149), we have determined a subnanometer-resolution structure for the WHV capsid by cryo-electron microscopy (cryo-EM) and compared the biophysical properties of HBV and WHV assembly. Cryo-EM reveals minimal differences in the structures of wCp149 and hCp149, which is in contrast to their assembly behaviors. Light scattering (LS) and size-exclusion chromatography (SEC) demonstrate rapid assembly and a strong association of wCp149 in response to ionic strength. Transmission electron microscopy (TEM) also reveals a significant population of abnormal "monster" particles and a dearth of T=3 capsids. While hCp149 assembly is steeply temperature dependent, wCp149 capsids form with a similar association energy over a broad temperature range. These data demonstrate that despite a high degree of structural homology, hepadnaviral core proteins are acutely responsive to primary sequence, allowing a wide range of assembly behaviors.

MATERIALS AND METHODS

Construction of a WHV Cp149 expression plasmid. The 450-bp WHV Cp149 DNA sequence (GenBank accession number DQ875458.1) was synthesized with 5′ NdeI and 3′ BamHI restriction sites (GenScript USA, Inc.). The WHV Cp149 gene was cloned into a pET11c expression plasmid and verified by both HindIII digestion analysis and sequencing. Successful clones were transformed into *Escherichia coli* BL21(DE3) cells.

Purification of hCp149 and wCp149. *E. coli* BL21 cells carrying a pET11c plasmid containing either the *adyw* strain of HBV Cp149 (GenBank accession number J02202.1) or WHV Cp149 were grown in Terrific broth medium containing 0.1 mg/ml carbenicillin overnight at 37°C and purified as described previously (32), with the following changes for the purification of wCp149.

After wCp149 purification on a Sepharose CL-4B column, capsid fractions were dialyzed against buffer N (50 mM $NaHCO_3$ [pH 9.5 at 4°C], 1 mM dithiothreitol [DTT]), and a portion of this material was stored directly at −80°C (*E. coli*-purified WHV capsids). The remaining capsids were disassembled by the addition of urea to a final concentration of 2 M and incubation at 4°C for 1 h. wCp149 dimers were purified on a Sephacryl S-300 column, pressure concentrated to 2 mg/ml (Millipore Corp., Bedford, MA), passed through a 0.22-μm filter, and stored at −80°C.

HBV Cp149 V124W and oxidized HBV Cp149 were prepared as described previously (31, 33).

Cp149 dimer preparation. Freshly thawed Cp149 dimers were prepared by dissociating any aggregates in 3 M urea at 4°C with mixing for 1.5 h, followed by dialysis against either 10 mM HEPES (pH 7.5 at 23°C) for wCp149 or 50 mM HEPES (pH 7.5 at 23°C) for hCp149. wCp149 dimers were quantified by using an ε_{280} of 65,840 M^{-1} cm^{-1}, and hCp149 dimers were quantified by using an ε_{280} of 60,900 M^{-1} cm^{-1}, based on the number of tryptophan and cysteine residues.

Cryo-electron microscopy. *E. coli*-purified WHV capsids were further purified on a Superose 6 10/300 GL column (GE Healthcare) with a running buffer containing 150 mM NaCl and 10 mM HEPES (pH 7.5). Capsids were concentrated by using 100-kDa cutoff Nanosep spin columns (Pall Corp.). The cryo-EM specimen was prepared by using an FEI Vitrobot instrument. Briefly, 4 μl of wCp149 capsids was applied onto a glow-discharged, holey, carbon-coated grid (R2/2; Quantifoil) for 25 s in 100% humidity. The grid was blotted with filter paper for 4 s and immediately plunged into a liquid nitrogen-cooled ethane bath. These vitrified specimens were maintained at −176°C in a Gatan 626DH cryo-holder during examination with a JEOL 3200FS electron microscope equipped with an in-column energy filter using a slit width of 20 eV. The microscope was operated at 300 kV under low-dose conditions (<25 $e^-/Å^2$). Images were recorded on a Gatan charge-coupled-device (CCD) camera (Ultrascan 4000) at a nominal magnification of ×80,000 (corresponding to 0.1484 nm/pixel) with a defocus level ranging from 1.1 to 3.3 μm (34).

Image analysis and three-dimensional reconstruction. Images of T=4 particles were extracted from micrographs by using a square box of 301 by 301 pixels using e2boxer.py (35). These particle files were then normalized and the power spectra were computed by using RobEM (http://cryoem.ucsd.edu/programs.shtm) to assess micrograph quality. Only data without drift or astigmatism were selected for image processing. The defocus estimation was carried out by using CTFFIND3 (36). An initial model was generated by using the *ab initio* random-model method (37, 38). The preliminary origin and orientation search was done iteratively by using a parallel polar Fourier transformation (PPFT) algorithm and further refined by PO^2R using the AUTO3DEM package. The resolution of the three-dimensional (3D) reconstruction was assessed by a Fourier shell correlation (FSC) of 0.5. The 3D reconstructions were rendered and visualized by using RobEM and UCSF Chimera (39). Chimera was also used to fit the atomic coordinates of the hCp149 capsid (PDB accession number 1QGT) into the cryo-EM electron density map of wCp149. To evaluate the structural homology between hCp149 and wCp149, a map based on atomic coordinates of the hCp149 capsid (PDB accession number 1QGT) was low-pass filtered to generate a 9.7-Å electron density map by using e2pdb2mrc.py (35). The FSC was calculated between this map and the wCp149 cryo-EM density map. The root mean square deviation (RMSD) between the atomic coordinates of the hCp149 capsid (PDB accession number 1QGT) and the molecular model of dimers rigid-body fit into wCp149 was calculated by using UCSF Chimera.

The wCp149 cryo-EM density map is now available in the EMDB as EMD-2692.

Ninety-degree light scattering of core protein assembly. Light scattering was monitored at 400 nm by using a QuantaMaster 40 fluorometer (Horiba Scientific) and a black-masked, 0.3-cm-path-length cuvette (Helma). Samples were monitored for ~50 s before diluting to the final assay conditions with an equal volume of 2× buffered NaCl to initiate assembly. Traces were synchronized to the time at which salt was first added to the reaction mixture.

Equilibration of wCp149 assembly. To define the equilibration time of wCp149 assembly, a series of assembly reaction mixtures containing 5 μM protein with 50, 100, 150, and 300 mM NaCl were allowed to equilibrate at room temperature. The amount of capsid formed was measured at 8-h intervals for the first 72 h with a final time point at 2 weeks. Samples were analyzed by SEC using a Superose 6 10/300 GL column. Peak areas of dimer and capsid were integrated by using Shimadzu LC Solutions software (Shimadzu Scientific Instruments).

Thermodynamics of wCp149 assembly. HBV capsid assembly has previously been described as a series of bimolecular reactions going from 120 dimers to a complete capsid particle (18, 22, 23):

$$120 \text{ dimers} \leftrightarrow \text{capsid} \tag{1}$$

At equilibrium, the association constant for the reaction can be defined as:

$$K_{\text{capsid}} = \frac{[\text{capsid}]}{[\text{dimer}]^{120}} \tag{2}$$

Given the inconvenient units of M^{-119} for K_{capsid}, equation 2 can be rewritten in terms of an association constant between two dimers:

$$K_{\text{capsid}} = \Pi_i s_i K_{\text{cont}}^{240} \tag{3}$$

where $\Pi_i s_i$ is a statistical term for the degeneracy of the reaction, equal to $2^{119}/120$, and the exponent of K_{cont} is for the number of contacts made in the complete virus capsid. From K_{cont}, Gibbs free energy of association between two dimers can be calculated as follows:

$$\Delta G_{\text{cont}} = -RT \ln(K_{\text{cont}}) \tag{4}$$

A pseudocritical concentration of assembly, $K_{D,\text{app}}$, can also be defined from K_{capsid} describing the concentration at which dimer and capsid are equal:

$$K_{D,\ \text{app}} = K_{\text{capsid}}^{(1/-119)} \tag{5}$$

These same principles were used to describe the thermodynamics of wCp149 assembly. To this end, salt-induced assembly reactions with either 50 or 100 mM NaCl using a range of wCp149 dimer concentrations from 0.5 to 20 μM were analyzed after 48 h at room temperature by SEC using a Superose 6 10/300 GL column. Since equilibration data indicated that wCp149 assembly reactions were not complete by 72 h of incubation, all thermodynamic parameters derived from this analysis are underestimates. The shorter time represents a compromise between reactions that were not fully equilibrated and reactions where damage to the protein (e.g., by oxidation) became significant issues (31).

Charge detection mass spectrometry. An assembly reaction mixture containing 40 μM wCp149 in 100 mM NaCl–10 mM HEPES (pH 7.5) was incubated for 48 h at room temperature before five dialyses against 250 ml of 100 mM ammonium acetate for 30 min each. The assembly sample was passed through a 0.22-μm filter. For some experiments, the sample was further purified by spin-column SEC (Bio-Rad Laboratories, Inc.) before charge detection mass spectrometry (CDMS) analysis. Detailed descriptions of the home-built mass spectrometer were reported previously (40–42). Briefly, the instrument passes a narrow band of ion energies into an ion trap for mass analysis. The ion's fundamental frequency of oscillation in the trap is used to deduce the mass-to-charge ratio (m/z). The magnitude of the fundamental peak in the fast Fourier transform is proportional to the charge. The mass is determined for each individual ion by multiplying m/z and z, and the compiled results are binned to form a mass spectrum. The absolute RMSD of z is approximately 1.5 electrons for the ~94-ms trapping time used here, and the relative RMSD of m/z is ~0.01, leading to an expected relative RMSD of mass of ~0.013 to 0.014.

Temperature-dependent assembly of wCp149 and hCp149. Assembly reaction mixtures containing 10 μM wCp149 in 100 mM NaCl–10 mM HEPES (pH 7.5 at 23°C) or 10 μM hCp149 in 300 mM NaCl–50 mM

HEPES (pH 7.5 at 23°C) were incubated at various temperatures between 4°C and 40°C for 48 h before analysis by SEC using a Superose 6 10/300 GL column mounted to a high-performance liquid chromatography (HPLC) system. All reagents were equilibrated to the assay temperature for 20 min before initiation of assembly by the addition of NaCl. Reaction mixtures were incubated in a Mastercycler Pro instrument (Eppendorf AG) with the heated lid function disabled. Reaction mixtures were maintained at the assay temperature within the autosampler chamber of the HPLC system during analysis.

Using equation 4 and the relation

$$\Delta G = \Delta H - T\Delta S \quad (6)$$

the amounts of capsid and dimer formed under each reaction condition can be related to temperature by the van't Hoff equation:

$$\ln(K_{\text{cont}}) = -\frac{\Delta H}{RT} + \frac{\Delta S}{R} \quad (7)$$

where R is the gas constant and T is the temperature in Kelvins. To account for the heat capacity temperature dependence of both enthalpy and entropy, equation 7 was expanded to the following relation (43):

$$\ln(K_{\text{cont}}) = -\frac{\Delta H_{T1} + \Delta C_p(T_2 - T_1)}{RT_2} + \frac{\Delta S_{T1} + \Delta C_p \ln\left(\frac{T_2}{T_1}\right)}{R} \quad (8)$$

where ΔC_p is the heat capacity of the assembly reaction. Values for ΔH, ΔS, and ΔC_p were determined by minimizing the root mean square deviation between calculated and experimental data.

Transmission electron microscopy. All samples were prepared on glow-discharged, 300-mesh, carbon-coated copper grids (EM Sciences) stained with 2% uranyl acetate. Micrographs were taken on a 4k × 4k CCD camera (Gatan), using a JEOL 1010 transmission electron microscope (IMBI Multidisciplinary Microscope Facility).

RESULTS

3D cryo-electron microscopy reconstruction of wCp149 capsids purified from *E. coli*. A C-terminally truncated version of the WHV core protein corresponding to the 149-residue assembly domain (wCp149) was expressed in *E. coli* and purified as described above. The 260-nm/280-nm absorbance ratio of capsids was 0.7, consistent with purified protein without contaminating nucleic acid (44).

Capsids were imaged by cryo-EM to generate a 3D reconstruction of a T=4 wCp149 capsid (Fig. 2). Micrographs of wCp149 capsids showed a mix of assembly products, including a predominance of T=4 icosahedral capsids and some large, ovate particles (Fig. 2A and 3D and E). T=3 capsids were also observed but at a much lower concentration than in HBV Cp149 (hCp149) preparations (0.3% and ~5 to 10%, respectively). Charge detection mass spectrometry (CDMS) verified the presence of large particles (data not shown). The desalting process, however, led to the depletion of these large particles, making the 4.2-MDa particles corresponding to T=4 symmetry the only species observed in most spectra (Fig. 3B). T=3 particles were undetectable in samples of wCp149.

To a first approximation, micrographs of WHV T=4 particles had few obvious differences from hCp149 capsids. When T=4 particles were averaged, a single band of density was present (Fig. 2A, inset); this is identical to the average of hCp149 capsids lacking RNA (34). A total of 2,254 T=4 particles from 133 micrographs were used to compute image reconstruction, starting from a random model. The resolution presented, based on a Fourier shell correlation of 0.5, is 9.7 Å. A surface-shaded representation of the wCp149 capsid reconstruction (Fig. 2B and C) was indistinguishable from that of T=4 hCp149 capsids (34). The capsid surface was dominated by 120 dimer spikes, each a four-helix bundle (16, 45). By convention, there are AB dimers and CD dimers. The five monomers surrounding the 5-fold vertices are A subunits, three CD dimers surround 3-fold axes, and two sequences of B, C, and D monomers surround the quasi-6-fold vertices. The density on the interior of the capsid showed no evidence for packaged nucleic acid.

To compare the wCp149 and hCp149 capsid structures, the 3.3-Å crystal structure of an hCp149 capsid (PDB accession number 1QGT) was manually fit into the wCp149 capsid EM density and refined by the Chimera "fit in map" function (Fig. 2B and D) (46). Overall, the structures agree remarkably well (Fig. 2E and F). An overlay of subunits from an HBV capsid and subunits fit into the wCp149 capsid density shows a very strong overlap in spite of the sequence differences and the modest resolution of the structures (Fig. 2F). The calculated RMSD between the structure of the hCp149 capsid (PDB accession number 1QGT) and the structure fit into wCp149 is ~0.785 Å for the whole asymmetric unit (Table 1). The spike that comprises the intradimer interface, the region with the greatest sequence divergence, exhibited slight inconsistencies. In particular, the hCp149 AB dimer extended outside the wCp149 EM density. Similarly, side chains of the D subunit also showed small mismatches (Fig. 2D). The sequence from residues 66 to 93 is particularly divergent (Fig. 1).

Kinetics and product morphologies of salt-induced wCp149 assembly. The assembly properties of hCp149 are well characterized. hCp149 assembly is sensitive to pH, temperature, and ionic strength (18, 19). Surprisingly, initial experiments showed that wCp149 formed capsids when stored in 50 mM HEPES buffer (pH 7.5), conditions where hCp149 is entirely dimeric even at relatively high concentrations (ca. 60 μM). wCp149 capsids were not observed when stored in 10 mM HEPES, suggesting that wCp149 assembled at a lower ionic strength than did hCp149.

To characterize the kinetics of capsid formation, the dependence of wCp149 and hCp149 assembly on ionic strength was systematically investigated by light scattering (LS) (Fig. 3A). The LS signal correlates with the number of particles in solution and their size, allowing particle formation to be monitored in real time. wCp149 exhibited robust assembly at NaCl concentrations as low as 50 mM. At higher salt concentrations, the LS signal rapidly plateaued, indicating that the reaction was either largely completed or kinetically trapped (24). It is also notable that the maximum LS signal continued to increase with increasing NaCl concentrations, suggesting that more capsids and/or larger aggregates were forming. Identical concentrations of hCp149 at the same ionic strengths showed no evidence of assembly even at 150 mM NaCl. At 300 mM NaCl, hCp149 assembly was evident but was much slower than that of wCp149 in 50 mM NaCl and did not reach the same extent.

To better understand the source of increased LS from wCp149 assemblies, the reaction products 48 h after induction of assembly were imaged by negative-stain transmission electron microscopy (TEM) (Fig. 3C to E). Comparison of micrographs from hCp149 and wCp149 reactions revealed two important differences consistent with and confirmed by light scattering (and chromatographic experiments [Fig. 4]). First, the same concentration of dimer protein produced more particles for wCp149 than for hCp149 under similar assembly conditions (compare Fig. 3C with D and E). Second, although wCp149 assembled into typical, well-formed T=4 capsids, some atypical capsids larger than T=4 with nonspherical

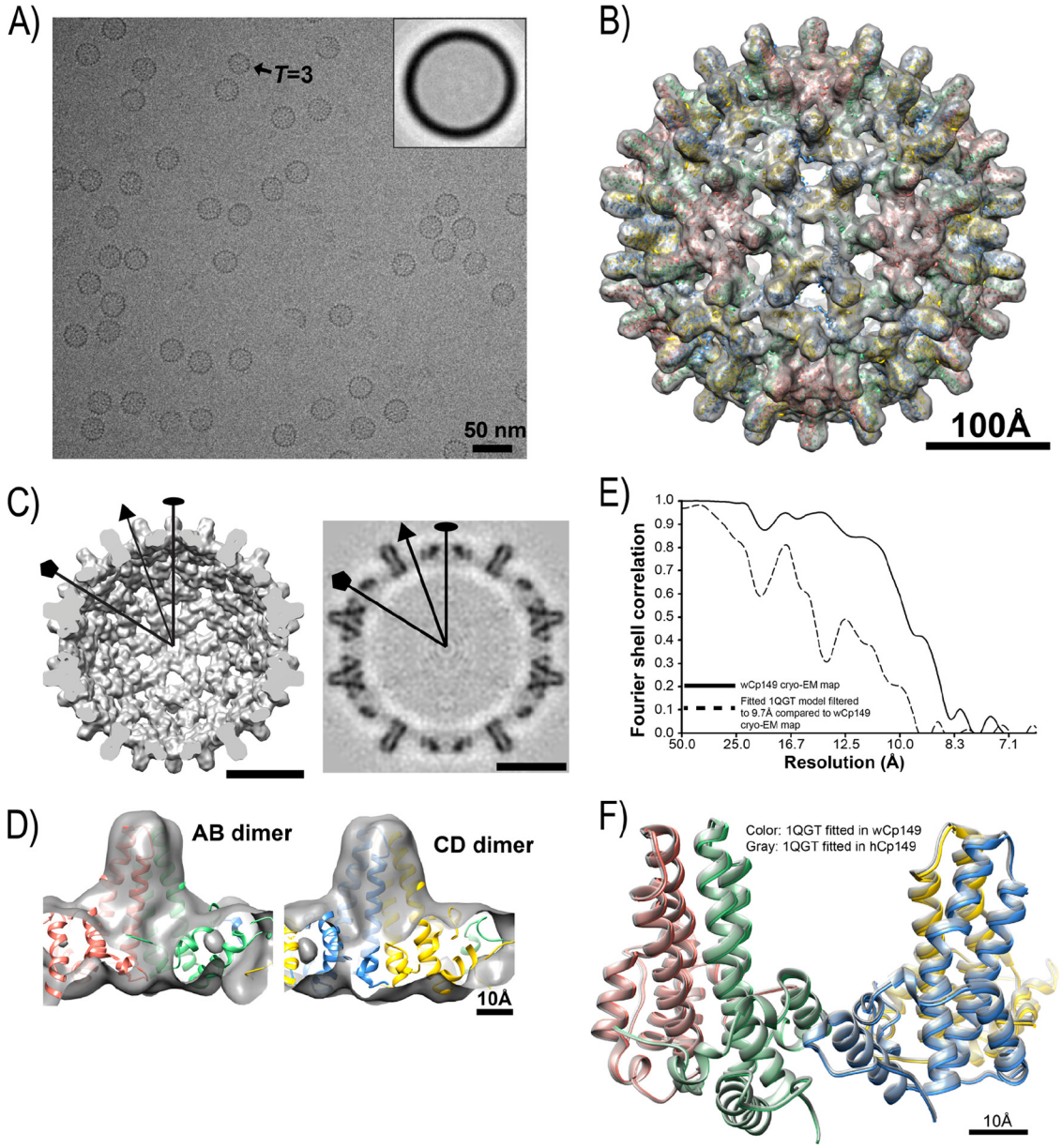

FIG 2 Cryo-EM 3D reconstruction of wCp149 capsids purified from *E. coli*. (A) Representative cryo-electron micrograph showing wCp149 capsids. An arrow identifies a rare T=3 particle. The inset shows a translationally aligned average image that has a single layer of capsid density. (B) Twofold view of the wCp149 capsid (transparent isosurface) fit with hCp149 dimers (PDB accession number 1QGT) (ribbon representation). A, B, C, and D quasiequivalent subunits are shown in red, green, blue, and yellow, respectively. (C, left) Isosurface representation of the capsid shell viewed along the 2-fold axis showing a smooth inner surface. (Right) Central section of the 3D reconstruction of the wCp149 capsid highlighting the absence of any internal density. Icosahedral 2-, 3-, and 5-fold symmetry axes are marked as ovals, triangles, and pentagons, respectively. Bar, 10 nm. (D) An AB dimer (left) and a CD dimer (right), viewed from the side, showing that the density of the structure reported under PDB accession number 1QGT fits well into the wCp149 capsid EM density. (E) The FSC resolution determined for the cryo-EM density map of wCp149 is 9.7 Å (solid line; FSC = 0.5 at this resolution). The FSC calculated between an HBV capsid low-pass filtered to 9.7 Å (calculated from 1QGT) and the wCp149 cryo-EM density map is 14.6 Å (dashed line). (F) An overlay of hCp149 dimers (1QGT) fit as rigid bodies into the wCp149 capsid density. In the overlays, the AB dimers are red-green and the CD dimers are yellow-blue, with hCp149 in transparent gray. RMSD calculations between wCp149 and hCp149 are shown in Table 1. The EMDB accession number for the wCp149 cryo-EM density map is EMD-2692.

morphology were also observed. These large capsids became more prevalent as NaCl concentrations were increased to ≥300 mM. Although rare, in some instances, double-layered particles were observed, reminiscent of cowpea chlorotic mosaic virus (CCMV) assemblies at low pH and low ionic strength (47, 48). In contrast to these observations, hCp149 assembly produced few deformed capsids; most corresponded to T=3 and T=4 particles (Fig. 3C) (42).

Thermodynamics of salt-induced wCp149 assembly. wCp149 assembly appeared to produce more capsids than did hCp149 reactions, suggesting that wCp149 was the energetically favored reaction. To obtain a quantitative description of its ener-

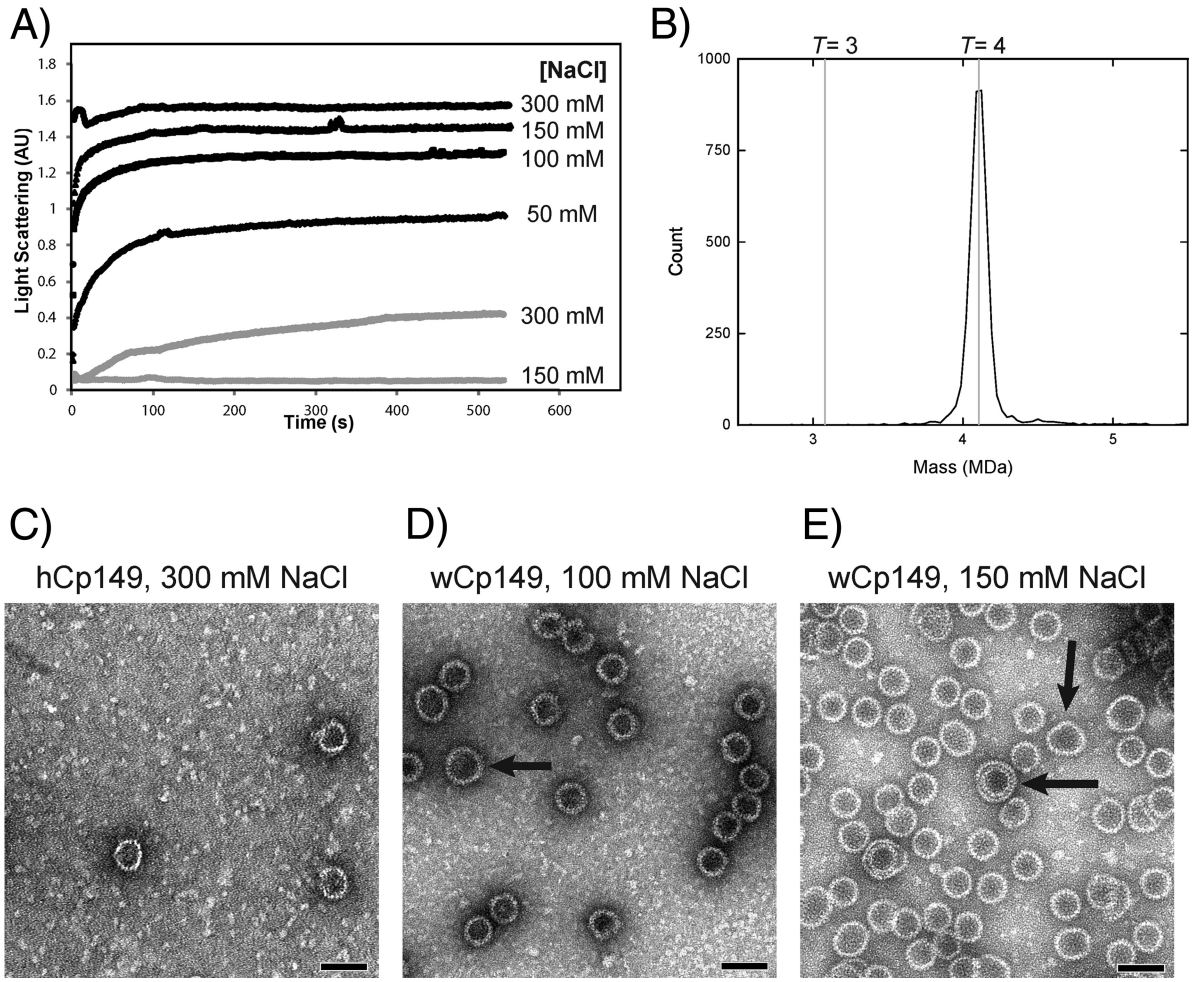

FIG 3 Salt-induced reactions of wCp149 assembled faster, to a greater extent, and at a lower ionic strength than hCp149. (A) Light scattering showing that assembly of 10 μM wCp149 (black) in 10 mM HEPES (pH 7.5) induced by the indicated NaCl concentrations was highly aggressive compared to hCp149 assembly (gray). The lines are the means of data from triplicate measurements. AU, arbitrary units. (B) Charge detection mass spectrometry of 40 μM wCp149 assembled in 100 mM NaCl for 48 h and then exchanged into 100 mM ammonium acetate by a desalting column. The gray lines in the spectrum indicate the expected location for a peak corresponding to a T=3 and a T=4 capsid. (C to E) Negative-stained electron micrographs of 10 μM hCp149 in 300 mM NaCl (C), 10 μM wCp149 in 100 mM NaCl (D), and 10 μM wCp149 in 150 mM NaCl (E) after 48 h at room temperature (magnification, ×60,000). Some atypically large capsids with unusual morphology are marked by black arrows. Bar, 50 nm.

getics, wCp149 assembly reactions were subjected to a thermodynamic analysis. Initial experiments, however, revealed that equilibration of wCp149 occurred on a much longer time scale than for hCp149, as measured by the amounts of capsid and dimer by SEC (Fig. 4A). Whereas most hCp149 assembly reactions equilibrate within 24 h (18, 27), wCp149 reactions had not reached equilibrium after 48 h at room temperature. Assembly reactions at 50 and 100 mM NaCl formed 10 to 15% more capsid after 2 weeks (336 h) of equilibration than at 72 h. In comparison, assembly reactions at 150 and 300 mM NaCl plateaued very quickly, reaching >90% capsid within a few hours. However, this plateau may reflect our limited ability to detect small changes in assembly reactions that are nearly quantitative. Furthermore, aggregates and misassembled intermediates observed previously (Fig. 3D and E) may not resolve chromatographically and may equilibrate very slowly (49). Therefore, all further characterization of wCp149 was performed with 100 mM NaCl or less.

TABLE 1 Structural comparison of models fit into HBV and WHV capsid densities

Segment(s)	RMSD electron density (Å)
A chain	0.85
B chain	0.73
C chain	0.75
D chain	0.81
All chains	0.79

To define thermodynamic parameters of wCp149 assembly, reactions at either 50 or 100 mM NaCl were measured after 48 h by using SEC to determine the amounts of capsid and dimer (Fig. 4B and Table 2). Although these reactions had not fully equilibrated at 48 h (Fig. 4A), longer incubations ran the risk of oxidative damage (31). Therefore, thermodynamic parameters derived from this analysis are underestimates. Plotting the amounts of free dimer and capsid versus the total amount of input protein revealed the expected pseudocritical concentration of assembly, or

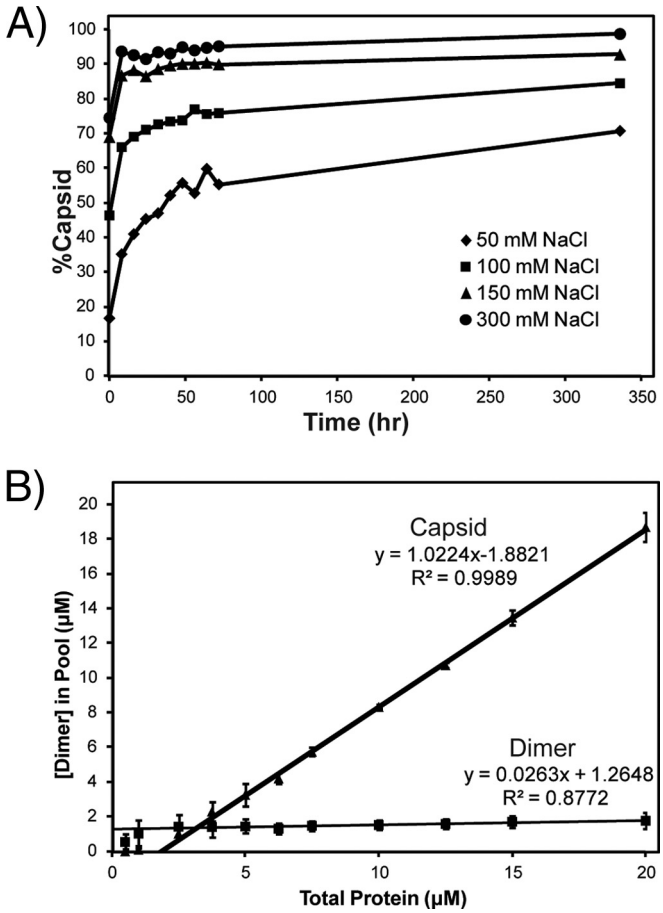

FIG 4 The wCp149 association is more favorable than that of hCp149. (A) Long-term assembly kinetics of wCp149 at room temperature observed over the course of 2 weeks at the indicated salt concentrations. The percentage of the total protein that formed capsid was quantified by SEC. Unlike hCp149, wCp149 assembly did not equilibrate within 24 h. (B) Assembly reaction mixtures of wCp149 were incubated in 100 mM NaCl for 48 h at room temperature before capsid and dimer amounts were quantified by SEC. The concentrations of wCp149 in the capsid and dimer pools showed a classic pseudocritical concentration of 1.8 μM (Table 2). Data points are the means ± standard deviations from triplicate measurements.

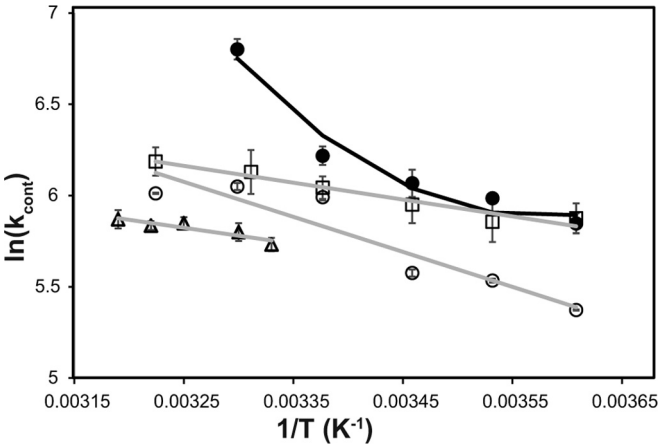

FIG 5 van't Hoff plot revealing that wCp149 capsid assembly (closed circles) displays nonlinear temperature dependence, unlike wt hCp149 and mutant variants (open symbols) (Table 3). The amounts of capsid and dimer formed after 48 h of assembly at temperatures between 4°C and 40°C were quantified by SEC. Buffer conditions were chosen so that easily measured quantities of capsid and dimer were present. Reaction mixtures contained 10 μM core protein in 100 mM NaCl–10 mM HEPES (wCp149 [filled circles]), 50 mM NaCl–50 mM HEPES (hCp149 V124W [empty squares]), or 300 mM NaCl–50 mM HEPES (wt hCp149 [empty circles] and oxidized hCp149 [empty triangles]). For wCp149, dimer concentrations were too low for quantification at 37°C, and for oxidized hCp149, reactions at temperatures below 27°C did not readily equilibrate. (Data for oxidized hCp149 are adapted from reference 31 with permission of the publisher.) Therefore, these data were excluded from the analysis. All data represent the means ± standard deviations from at least three measurements. For some data points, the markers occlude the error bars. The data for wCp149 were fit with equation 8, giving an RMSD of 0.07.

$K_{D,app}$ (Fig. 4B). Above this limit, virtually all additional dimers will go toward the formation of capsid (18). $K_{D,app}$ can be defined by extrapolating the linear region of the capsid concentration to the *x* intercept (33). Based on the *x* intercept, $K_{D,app}$ values of 3.1 ± 0.5 μM and 1.8 ± 0.7 μM were obtained for wCp149 in 50 and 100 mM NaCl, respectively. In comparison, hCp149 assembly at 100 mM NaCl exhibits a $K_{D,app}$ of 43.3 ± 5.0 μM (33).

TABLE 2 Thermodynamic parameters of variant core proteins at 23°C[a]

Protein	Mean $K_{D,app}$ (μM) ± SD	Mean ΔG_{cont} (kcal/mol) ± SD
wCp149	1.8 ± 0.7	−3.7 ± 0.1
hCp149[b]	43.3 ± 5.0	−2.7 ± 0.04
hCp149 V124W[b]	1.0 ± 0.4	−3.8 ± 0.1
wCp149 (50 mM NaCl)	3.1 ± 0.5	−3.6 ± 0.2
hCp149 (300 mM NaCl)[c]	1.9	−3.7 ± 0.2

[a] All data are from assembly reactions with 100 mM NaCl except where noted.
[b] See reference 33.
[c] See reference 18.

The contact energy between two dimers, ΔG_{cont}, was calculated by assuming that the 240 intersubunit contacts found in a T=4 particle are equivalent (18, 24, 50). A comparison of the thermodynamic parameters of wCp149 and hCp149 assembly is given in Table 2. These analyses agree with observations by LS and TEM showing that at the same ionic strength, the assembly of wCp149 is more thermodynamically favored than is the assembly of hCp149.

Temperature dependence of wCp149 reveals a positive heat capacity. To obtain a better understanding of the physical basis of the assembly differences between wCp149 and hCp149, we examined the temperature dependence of assembly, using van't Hoff analysis to determine the enthalpy (ΔH) of the reaction. For wCp149 and hCp149, the surface buried at interdimer contacts is largely hydrophobic. Burial of the hydrophobic surface is characterized by positive ΔH, positive entropy (ΔS), and negative heat capacity (ΔC_p), consistent with the release of a hydrating layer of water. Thus, we anticipated a steep temperature dependence of assembly, as observed for hCp149 (18).

To make the energetics of assembly comparable for both viruses, we assembled hCp149 in 300 mM NaCl and wCp149 in 100 mM NaCl (Table 2). The equilibrium constants of the wCp149 and hCp149 assembly reactions were quantified from the amounts of capsid and dimer formed after 48 h at several temperatures (Fig. 5). As expected, a positive ΔH was observed for the assembly of hCp149, consistent with previous measure-

TABLE 3 Enthalpic and entropic contributions to wCp149 and hCp149 assembly reveal a strongly endothermic reaction for woodchuck core proteins[a]

Parameter	Value for protein				
	wCp149 (100 mM NaCl)	hCp149 (300 mM NaCl)	hCp149 F97L (150 mM NaCl)[b]	hCp149 V124W (50 mM NaCl)	Oxidized hCp149 (300 mM NaCl)[c]
ΔG_{cont} (kcal/mol)	−3.7	−3.7	−3.0	−3.5	−3.4
ΔH (kcal/mol)	+8.9	+3.8	+7.4	+1.8	+1.8
$T\Delta S$ (kcal/mol)	+12.6	+7.5	+10.4	+5.3	+5.1
ΔS (cal/[mol · K])	+42.7	+25.4	+35.1	+18.0	+17.5
ΔC_p (cal/[mol · K])	+650	~0	ND	~0	~0

[a] ΔG values are for 23°C at the indicated salt concentrations. ND, not determined.
[b] See reference 27.
[c] Values adapted from reference 31 with permission of the publisher.

ments (Table 3) (18). The change in ΔH was approximately linear with $1/T$. Using the experimentally derived value for ΔG_{cont}, we found a positive ΔS for hCp149 assembly.

The temperature dependence of wCp149 assembly was more complicated. First, quantification of the amount of wCp149 dimer was not possible at temperatures of >30°C, since almost all of the protein had assembled. Second, the assembly trend for wCp149 displayed significant curvature, indicating that ΔH and ΔS were changing with temperature. The dependence of ΔH and ΔS on temperature is a function of ΔC_p. While ΔH and ΔS of wCp149 were also positive, they were much higher than those for hCp149 assembly (Table 3). Additionally, the curvature of the wCp149 assembly data allowed us to calculate a large, positive ΔC_p value of 670 ± 160 cal/(mol · K). The positive ΔC_p provides a physical basis for favorable assembly even at lower temperatures. The same analysis applied to hCp149 assembly yielded ΔC_p values indistinguishable from zero.

DISCUSSION

Core protein is highly dynamic, and its assembly is responsive to solution conditions (18–20, 30, 31, 51). Previous studies have revealed an intricate relationship between the structure and assembly properties of HBV core proteins (27, 29, 30, 33, 51, 52). Several small molecules that allosterically influence core protein assembly have been identified (32, 53–59). Given the considerable sequence similarity of WHV (Fig. 1), it was suspected that the core proteins from this virus would behave similarly to HBV.

Cryo-EM image reconstruction of the WHV capsid shows that it is nearly identical to the HBV capsid (Fig. 2). WHV has T=4 icosahedral symmetry and is comprised of 120 dimers. Mass measurement by CDMS is consistent with this assignment. The fit of the hCp149 capsid crystal structure to the image reconstruction density provides a further indication of the remarkable similarity between these two proteins (Fig. 2 and Table 1). Slight differences between the model and the density at the spike correlate with primary sequence differences (Fig. 1A and 2D and F). The overall root mean square displacement of the hCp149 two-dimer asymmetric unit from the highest-resolution HBV structure (PDB accession number 1QGT) to a rigid-body fit of dimers into the wCp149 capsid density is only 0.79 Å, indicating that even with the differences in the molecular envelope, there is tremendous agreement between the structures. The rarity of T=3 particles in wCp149 preparations based on microscopy and CDMS is an indication that seemingly innocuous sequence differences can have profound structural effects (Fig. 2A and 3B). At this resolution, however, there is no obvious structural explanation for the differences in wCp149 and hCp149 assembly.

The morphology of *in vitro*-assembled wCp149 presents another striking feature. TEM images of wCp149 assembly revealed a predominance of T=4 particles with a notable presence of larger, nonspherical structures (Fig. 3D and E). These abnormal products may represent kinetically trapped, off-path intermediates, which correlates well with the high ΔG_{cont} and faster assembly kinetics of wCp149 (23). LS data imply a significant role for assembly kinetics in the formation of these atypical capsids. Assembly reactions of wCp149 in 100 mM NaCl and of hCp149 in 300 mM NaCl have similar ΔG_{cont} values, but the wCp149 reaction occurs much faster (Fig. 3A). Abnormally large products suggest that wCp149 can adopt different geometries at dimer-dimer contacts. Consistent with flexible geometry, micrographs revealed occasional double-layered particles, where it appears that a T=4 capsid has nucleated the formation of an outer shell (Fig. 3E). These aberrant wCp149 capsids are the subject of further investigation. Similar multilayered shells have been observed for CCMV assembly (47, 60). In contrast, hCp149 assembly produces few overlarge capsids even at NaCl concentrations as high as 1 M (Fig. 3C) (42). The formation of atypical capsids is a property of wCp149 dimers and not exclusively an effect of their sensitivity to ionic strength. hCp149 can be induced to form aberrant particles by point mutations such as V124F (Z. Tan, K. Pionek, N. Unchwaniwala, M. L. Maguire, D. D. Loeb, and A. Zlotnick, submitted for publication), small molecules (32, 59), or an N-terminal extension (61). Thus, assignment of the differences in wCp149 and hCp149 to any of the 52 sequence differences is not trivial.

Light scattering, size-exclusion chromatography, and transmission electron microscopy were used to characterize and quantify the assembly of wCp149. LS demonstrated that wCp149 assembled faster, to a greater extent, and at a lower ionic strength than hCp149 (Fig. 3A). The difference in assembly was quantified in terms of ΔG_{cont} (Fig. 4B and Table 2). Under identical conditions of ionic strength, wCp149 exhibited a 1.0-kcal/mol-higher ΔG_{cont}, corresponding to a 24-fold-lower $K_{D,app}$, than that of hCp149.

To understand the basis for the difference in wCp149 and hCp149 behaviors, we examined the temperature dependence of assembly. We were surprised at the drastic difference in the temperature-dependent assembly of these two core proteins, which was observed under conditions where wCp149 and hCp149 had similar association energies (Fig. 5 and Table 3). wCp149 assembly remained highly favorable at temperatures as low as 4°C (>60% of

capsids), unlike hCp149 (<5% of capsids). Both ΔH and ΔS were higher for wCp149 assembly. While hCp149 assembly remained fairly linear with temperature, wCp149 showed a significant curvature in its temperature-dependent assembly, indicating a high and positive ΔC_p of 670 ± 160 cal/(mol · K). Single mutations of hCp149, which either strengthen association energy to magnitudes comparable to those of wCp149 (e.g., V124W) or weaken association energy (C61-C61 disulfide cross-linking), have no effect on heat capacity (Fig. 5 and Table 3). These observations reinforce that the unique assembly properties of wCp149 may not result from a single-residue change but rather may be the product of several amino acids acting in concert to achieve balanced and robust capsid formation.

The energetic differences between wCp149 and hCp149 assembly have profound implications for understanding core protein in solution. We propose that the energetic differences between hCp149 and wCp149 result from structural and/or dynamic differences in the free dimer. In HBV capsids, dimers are held together by a hydrophobic contact. Based on sequence and structural similarity, we expect (but have not found) a similar behavior for wCp149. Classically, burial of the hydrophobic surface is characterized by a positive ΔS, a positive ΔH, and a negative ΔC_p, consistent with the release of the waters that surround the hydrophobic patch into the bulk solvent. However, hCp149 has a ΔC_p near zero and wCp149 has a ΔC_p of assembly that is high and positive, inconsistent with the burial of the hydrophobic surface by the association of two rigid bodies, but what if the free dimer is dynamic? The large differences in ΔH and ΔS for hCp149 and wCp149 are similar to the differences between wild-type (wt) hCp149 and the hCp149 F97L mutant (Table 2), a mutation at the intradimer interface far from the site of interdimer contact (27). We observed that hCp149 free dimer structures show tremendous diversity (62), which may indicate that the free dimer is actually an ensemble of conformations (63, 64). Indeed, several lines of evidence indicate that HBV assembly involves a conformational change of the dimer from an assembly-inactive to an assembly-active state (18, 30, 31, 51, 52). Thus, we propose that the energetic differences between hCp149 and wCp149 indicate that there are structural or dynamic differences in the free dimer. In this situation, the net energy of assembly includes the costs of the transition from the inactive to the active state, which we propose to be very different for wCp149 and hCp149 dimers.

We suggest that there is a biological advantage to the positive ΔC_p, which dampens the effects of temperature on capsid assembly. Woodchucks are hibernating mammals whose body temperatures range from 37°C during normal activity to as low as 6.5°C during periods of hibernation (65). During its normal activity and in response to environmental stress, woodchuck daily body temperatures fluctuate by as much as 14°C. Thus, a positive ΔC_p is an evolutionary advantage to a virus such as WHV but is not advantageous to viruses of thermally homeostatic animals such as humans. We speculate that a positive ΔC_p will be a feature common to viruses that must be active over a very broad range of temperatures, as in hibernating animals.

In this study, we examine the biophysics of WHV capsid assembly and WHV structure. The structures of the WHV and HBV capsids are very similar, but the thermodynamics of assembly are very different. Additionally, *in vitro* assembly reveals a multitude of abnormal structures not observed in hCp149 reactions. These data led us to propose that the free dimers of the two proteins have structural and/or dynamic differences not evident in the structure of an assembled capsid. The energetic differences allow wCp149 to assemble quickly over a broad temperature range that is peculiarly suited for a hibernating animal. This study has opened a window on the assembly of a virus adapted to a nonisothermal environment, providing depth in the complexity with which self-assembling proteins evolve. There may be parallels in the thermodynamics of assembly for plant viruses and viruses whose life cycles include transmission through insect vectors.

ACKNOWLEDGMENTS

This work was supported by NIH grant R01-AI077688 to A.Z and by NSF award 0832651 to M.F.J.

We thank David Nickens for his advice and suggestions. We also recognize the Electron Microscopy Center at Indiana University.

A.Z. reports a potential conflict of interest related to an interest in a company based on assembly effectors.

REFERENCES

1. **Beasley RP, Alter HJ, Brandeau ML, Church DR, Evans AA, Hagan H, Hullet S, Maroushek SR, Mayer RR, McMahon BJ, Sepulveda MJ, So S, Thomas DL, Wright LN.** 2010. Hepatitis and liver cancer: a national strategy for prevention and control of hepatitis B and C. National Academies Press, Washington, DC.
2. **Seeger C, Zoulim F, Mason WS.** 2007. Hepadnaviruses, p 2977–3029. *In* Knipe DM, Howley PM, Griffin DE, Lamb RA, Martin MA, Roizman B, Straus SE (ed), Fields virology, 5th ed, vol 2. Lippincott Williams & Wilkins, Philadelphia, PA.
3. Reference deleted.
4. **Ferir G, Kaptein S, Neyts J, De Clercq E.** 2008. Antiviral treatment of chronic hepatitis B virus infections: the past, the present and the future. Rev. Med. Virol. **18:**19–34. http://dx.doi.org/10.1002/rmv.554.
5. **Grimm D, Thimme R, Blum HE.** 2011. HBV life cycle and novel drug targets. Hepatol. Int. **5:**644–653. http://dx.doi.org/10.1007/s12072-011-9261-3.
6. **Tenney DJ, Levine SM, Rose RE, Walsh AW, Weinheimer SP, Discotto L, Plym M, Pokornowski K, Yu CF, Angus P, Ayres A, Bartholomeusz A, Sievert W, Thompson G, Warner N, Locarnini S, Colonno RJ.** 2004. Clinical emergence of entecavir-resistant hepatitis B virus requires additional substitutions in virus already resistant to lamivudine. Antimicrob. Agents Chemother. **48:**3498–3507. http://dx.doi.org/10.1128/AAC.48.9.3498-3507.2004.
7. **Torresi J, Earnest-Silveira L, Deliyannis G, Edgtton K, Zhuang H, Locarnini SA, Fyfe J, Sozzi T, Jackson DC.** 2002. Reduced antigenicity of the hepatitis B virus HBsAg protein arising as a consequence of sequence changes in the overlapping polymerase gene that are selected by lamivudine therapy. Virology **293:**305–313. http://dx.doi.org/10.1006/viro.2001.1246.
8. **Zoulim F, Locarnini S.** 2009. Hepatitis B virus resistance to nucleos(t)ide analogues. Gastroenterology **137:**1593–1608 e1591–1592. http://dx.doi.org/10.1053/j.gastro.2009.08.063.
9. **Kulkarni K, Jacobson IM, Tennant BC.** 2007. The role of the woodchuck model in the treatment of hepatitis B virus infection. Clin. Liver Dis. **11:**707–725. http://dx.doi.org/10.1016/j.cld.2007.08.012.
10. **Menne S, Cote PJ.** 2007. The woodchuck as an animal model for pathogenesis and therapy of chronic hepatitis B virus infection. World J. Gastroenterol. **13:**104–124. http://dx.doi.org/10.3748/wjg.v13.i1.104.
11. **Tennant BC, Gerin JL.** 2001. The woodchuck model of hepatitis B virus infection. ILAR J. **42:**89–102. http://dx.doi.org/10.1093/ilar.42.2.89.
12. **Nassal M.** 2008. Hepatitis B viruses: reverse transcription a different way. Virus Res. **134:**235–249. http://dx.doi.org/10.1016/j.virusres.2007.12.024.
13. **Schädler S, Hildt E.** 2009. HBV life cycle: entry and morphogenesis. Viruses **1:**185–209. http://dx.doi.org/10.3390/v1020185.
14. **Seeger C, Mason WS.** 2000. Hepatitis B virus biology. Microbiol. Mol. Biol. Rev. **64:**51–68. http://dx.doi.org/10.1128/MMBR.64.1.51-68.2000.
15. **Yan H, Zhong G, Xu G, He W, Jing Z, Gao Z, Huang Y, Qi Y, Peng B, Wang H, Fu L, Song M, Chen P, Gao W, Ren B, Sun Y, Cai T, Feng X, Sui J, Li W.** 2012. Sodium taurocholate cotransporting polypeptide is a

functional receptor for human hepatitis B and D virus. eLife **1:**e00049. http://dx.doi.org/10.7554/eLife.00049.
16. **Crowther RA, Kiselev NA, Bottcher B, Berriman JA, Borisova GP, Ose V, Pumpens P.** 1994. Three-dimensional structure of hepatitis B virus core particles determined by electron cryomicroscopy. Cell **77:**943–950. http://dx.doi.org/10.1016/0092-8674(94)90142-2.
17. **Nassal M.** 1992. The arginine-rich domain of the hepatitis B virus core protein is required for pregenome encapsidation and productive viral positive-strand DNA synthesis but not for virus assembly. J. Virol. **66:**4107–4116.
18. **Ceres P, Zlotnick A.** 2002. Weak protein-protein interactions are sufficient to drive assembly of hepatitis B virus capsids. Biochemistry **41:**11525–11531. http://dx.doi.org/10.1021/bi0261645.
19. **Wingfield PT, Stahl SJ, Williams RW, Steven AC.** 1995. Hepatitis core antigen produced in Escherichia coli: subunit composition, conformational analysis, and in vitro capsid assembly. Biochemistry **34:**4919–4932. http://dx.doi.org/10.1021/bi00015a003.
20. **Zlotnick A, Cheng N, Conway JF, Booy FP, Steven AC, Stahl SJ, Wingfield PT.** 1996. Dimorphism of hepatitis B virus capsids is strongly influenced by the C-terminus of the capsid protein. Biochemistry **35:**7412–7421. http://dx.doi.org/10.1021/bi9604800.
21. **Kenney JM, von Bonsdorff CH, Nassal M, Fuller SD.** 1995. Evolutionary conservation in the hepatitis B virus core structure: comparison of human and duck cores. Structure **3:**1009–1019. http://dx.doi.org/10.1016/S0969-2126(01)00237-4.
22. **Endres D, Zlotnick A.** 2002. Model-based analysis of assembly kinetics for virus capsids or other spherical polymers. Biophys. J. **83:**1217–1230. http://dx.doi.org/10.1016/S0006-3495(02)75245-4.
23. **Zlotnick A.** 1994. To build a virus capsid. An equilibrium model of the self assembly of polyhedral protein complexes. J. Mol. Biol. **241:**59–67.
24. **Zlotnick A, Johnson JM, Wingfield PW, Stahl SJ, Endres D.** 1999. A theoretical model successfully identifies features of hepatitis B virus capsid assembly. Biochemistry **38:**14644–14652. http://dx.doi.org/10.1021/bi991611a.
25. **Singh S, Zlotnick A.** 2003. Observed hysteresis of virus capsid disassembly is implicit in kinetic models of assembly. J. Biol. Chem. **278:**18249–18255. http://dx.doi.org/10.1074/jbc.M211408200.
26. Reference deleted.
27. **Ceres P, Stray SJ, Zlotnick A.** 2004. Hepatitis B virus capsid assembly is enhanced by naturally occurring mutation F97L. J. Virol. **78:**9538–9543. http://dx.doi.org/10.1128/JVI.78.17.9538-9543.2004.
28. **Yuan TT, Sahu GK, Whitehead WE, Greenberg R, Shih C.** 1999. The mechanism of an immature secretion phenotype of a highly frequent naturally occurring missense mutation at codon 97 of human hepatitis B virus core antigen. J. Virol. **73:**5731–5740.
29. **Yuan TT, Shih C.** 2000. A frequent, naturally occurring mutation (P130T) of human hepatitis B virus core antigen is compensatory for immature secretion phenotype of another frequent variant (I97L). J. Virol. **74:**4929–4932. http://dx.doi.org/10.1128/JVI.74.10.4929-4932.2000.
30. **Packianathan C, Katen SP, Dann CE, III, Zlotnick A.** 2010. Conformational changes in the hepatitis B virus core protein are consistent with a role for allostery in virus assembly. J. Virol. **84:**1607–1615. http://dx.doi.org/10.1128/JVI.02033-09.
31. **Selzer L, Katen SP, Zlotnick A.** 2014. The hepatitis B virus core protein intradimer interface modulates capsid assembly and stability. Biochemistry **53:**5496–5504. http://dx.doi.org/10.1021/bi500732b.
32. **Zlotnick A, Ceres P, Singh S, Johnson JM.** 2002. A small molecule inhibits and misdirects assembly of hepatitis B virus capsids. J. Virol. **76:**4848–4854. http://dx.doi.org/10.1128/JVI.76.10.4848-4854.2002.
33. **Tan Z, Maguire ML, Loeb DD, Zlotnick A.** 2013. Genetically altering the thermodynamics and kinetics of hepatitis B virus capsid assembly has profound effects on virus replication in cell culture. J. Virol. **87:**3208–3216. http://dx.doi.org/10.1128/JVI.03014-12.
34. **Wang JC, Dhason MS, Zlotnick A.** 2012. Structural organization of pregenomic RNA and the carboxy-terminal domain of the capsid protein of hepatitis B virus. PLoS Pathog. **8:**e1002919. http://dx.doi.org/10.1371/journal.ppat.1002919.
35. **Tang G, Peng L, Baldwin PR, Mann DS, Jiang W, Rees I, Ludtke SJ.** 2007. EMAN2: an extensible image processing suite for electron microscopy. J. Struct. Biol. **157:**38–46. http://dx.doi.org/10.1016/j.jsb.2006.05.009.
36. **Mindell JA, Grigorieff N.** 2003. Accurate determination of local defocus and specimen tilt in electron microscopy. J. Struct. Biol. **142:**334–347. http://dx.doi.org/10.1016/S1047-8477(03)00069-8.
37. **Yan X, Dryden KA, Tang J, Baker TS.** 2007. Ab initio random model method facilitates 3D reconstruction of icosahedral particles. J. Struct. Biol. **157:**211–225. http://dx.doi.org/10.1016/j.jsb.2006.07.013.
38. **Yan X, Sinkovits RS, Baker TS.** 2007. AUTO3DEM—an automated and high throughput program for image reconstruction of icosahedral particles. J. Struct. Biol. **157:**73–82. http://dx.doi.org/10.1016/j.jsb.2006.08.007.
39. **Pettersen EF, Goddard TD, Huang CC, Couch GS, Greenblatt DM, Meng EC, Ferrin TE.** 2004. UCSF Chimera—a visualization system for exploratory research and analysis. J. Comput. Chem. **25:**1605–1612. http://dx.doi.org/10.1002/jcc.20084.
40. **Contino NC, Jarrold MF.** 2013. Charge detection mass spectrometry for single ions with a limit of detection of 30 charges. Int. J. Mass Spectrom. **345–347:**153–159. http://dx.doi.org/10.1016/j.ijms.2012.07.010.
41. **Contino NC, Pierson EE, Keifer DZ, Jarrold MF.** 2013. Charge detection mass spectrometry with resolved charge states. J. Am. Soc. Mass Spectrom. **24:**101–108. http://dx.doi.org/10.1007/s13361-012-0525-5.
42. **Pierson EE, Keifer DZ, Contino NC, Jarrold MF.** 2013. Probing higher order multimers of pyruvate kinase with charge detection mass spectrometry. Int. J. Mass Spectrom. **337:**50–56. http://dx.doi.org/10.1016/j.ijms.2013.01.002.
43. **Fersht A.** 1999. Structure and mechanism in protein science: a guide to enzyme catalysis and protein folding. WH Freeman, New York, NY.
44. **Porterfield JZ, Zlotnick A.** 2010. A simple and general method for determining the protein and nucleic acid content of viruses by UV absorbance. Virology **407:**281–288. http://dx.doi.org/10.1016/j.virol.2010.08.015.
45. **Caspar DLD, Klug A.** 1962. Physical principles in the construction of regular viruses. Cold Spring Harb. Symp. Quant. Biol. **27:**1–24. http://dx.doi.org/10.1101/SQB.1962.027.001.005.
46. **Wynne SA, Crowther RA, Leslie AG.** 1999. The crystal structure of the human hepatitis B virus capsid. Mol. Cell **3:**771–780. http://dx.doi.org/10.1016/S1097-2765(01)80009-5.
47. **Adolph KW, Butler PJ.** 1976. Assembly of a spherical plant virus. Philos. Trans. R. Soc. Lond. B Biol. Sci. **276:**113–122. http://dx.doi.org/10.1098/rstb.1976.0102.
48. **Bancroft JB.** 1970. The self-assembly of spherical plant viruses. Adv. Virus Res. **16:**99–134. http://dx.doi.org/10.1016/S0065-3527(08)60022-6.
49. **Zlotnick A.** 2007. Distinguishing reversible from irreversible virus capsid assembly. J. Mol. Biol. **366:**14–18. http://dx.doi.org/10.1016/j.jmb.2006.11.034.
50. **Katen SP, Zlotnick A.** 2009. Thermodynamics of virus capsid assembly. Methods Enzymol. **455:**395–417. http://dx.doi.org/10.1016/S0076-6879(08)04214-6.
51. **DiMattia MA, Watts NR, Stahl SJ, Grimes JM, Steven AC, Stuart DI, Wingfield PT.** 2013. Antigenic switching of hepatitis B virus by alternative dimerization of the capsid protein. Structure **21:**133–142. http://dx.doi.org/10.1016/j.str.2012.10.017.
52. **Bourne CR, Katen SP, Fulz MR, Packianathan C, Zlotnick A.** 2009. A mutant hepatitis B virus core protein mimics inhibitors of icosahedral capsid self-assembly. Biochemistry **48:**1736–1742. http://dx.doi.org/10.1021/bi801814y.
53. **Bourne C, Lee S, Venkataiah B, Lee A, Korba B, Finn MG, Zlotnick A.** 2008. Small-molecule effectors of hepatitis B virus capsid assembly give insight into virus life cycle. J. Virol. **82:**10262–10270. http://dx.doi.org/10.1128/JVI.01360-08.
54. Reference deleted.
55. Reference deleted.
56. **Li L, Chirapu SR, Finn MG, Zlotnick A.** 2013. Phase diagrams map the properties of antiviral agents directed against hepatitis B virus core assembly. Antimicrob. Agents Chemother. **57:**1505–1508. http://dx.doi.org/10.1128/AAC.01766-12.
57. **Stray SJ, Bourne CR, Punna S, Lewis WG, Finn MG, Zlotnick A.** 2005. A heteroaryldihydropyrimidine activates and can misdirect hepatitis B virus capsid assembly. Proc. Natl. Acad. Sci. U. S. A. **102:**8138–8143. http://dx.doi.org/10.1073/pnas.0409732102.
58. **Stray SJ, Ceres P, Zlotnick A.** 2004. Zinc ions trigger conformational change and oligomerization of hepatitis B virus capsid protein. Biochemistry **43:**9989–9998. http://dx.doi.org/10.1021/bi049571k.
59. Reference deleted.
60. **Lavelle L, Gingery M, Phillips M, Gelbart WM, Knobler CM, Cadena-Nava RD, Vega-Acosta JR, Pinedo-Torres LA, Ruiz-Garcia J.** 2009. Phase diagram of self-assembled viral capsid protein polymorphs. J. Phys. Chem. B **113:**3813–3819. http://dx.doi.org/10.1021/jp8079765.
61. **Watts NR, Conway JF, Cheng N, Stahl SJ, Steven AC, Wingfield PT.** 2011. Role of the propeptide in controlling conformation and assembly

state of hepatitis B virus e-antigen. J. Mol. Biol. **409:**202–213. http://dx.doi.org/10.1016/j.jmb.2011.03.049.
62. Reference deleted.
63. **Bereszczak JZ, Watts NR, Wingfield PT, Steven AC, Heck AJ.** 2014. Assessment of differences in the conformational flexibility of hepatitis B virus core-antigen and e-antigen by hydrogen deuterium exchange-mass spectrometry. Protein Sci. **23:**884–896. http://dx.doi.org/10.1002/pro.2470.
64. **Hilmer JK, Zlotnick A, Bothner B.** 2008. Conformational equilibria and rates of localized motion within hepatitis B virus capsids. J. Mol. Biol. **375:**581–594. http://dx.doi.org/10.1016/j.jmb.2007.10.044.
65. **Zervanos SM, Salsbury CM.** 2003. Seasonal body temperature fluctuations and energetic strategies in free-ranging eastern woodchucks (Marmota monax). J. Mammal. **84:**299–310. http://dx.doi.org/10.1644/1545-1542(2003)084<0299:SBTFAE>2.0.CO;2.